Front. Phys. 10, 107403 (2015)
DOI 10.1007/s11467-015-0495-8

RESEARCH ARTICLE

Electronic and magnetic structures of ternary iron telluride KFe_2Te_2

Xu-Guang Xu, Wei Li†

State Key Laboratory of Functional Materials for Informatics and Shanghai Center for Superconductivity, Shanghai Institute of Microsystem and Information Technology, Chinese Academy of Sciences, Shanghai 200050, China

Corresponding author. E-mail: †liwei@mail.sim.ac.cn

Received May 15, 2015; accepted May 22, 2015

We examine the electronic and magnetic structures of iron telluride KFe_2Te_2 using first-principle calculations. We demonstrate that the ground state of this compound is in bicollinear antiferromagnetic order with Fe local moments ($\sim 2.6\ \mu_B$) that are ferromagnetically aligned along a diagonal direction and antiferromagnetically aligned along the other diagonal in the Fe-Fe square lattice, similar to the alignment discovered in the parent compound of superconductor α-FeTe. This bicollinear antiferromagnetic order results from the interplay among the nearest, next-nearest, and next-next-nearest neighbor exchange interactions, which are mediated by Te $5p$ orbitals. This finding may aid our understanding of the interplay between magnetism and superconductivity in the family of iron-based materials.

Keywords iron-basel materials, electronic and magnetic structures

PACS numbers 74.25.Jb, 74.70.-b, 74.25.Ha, 71.20.-b

Frontiers of Physics

1 Introduction

The search for high-temperature superconductivity and a novel superconducting mechanism is one of the most challenging tasks undertaken by condensed-matter physicists and material scientists. Since the discovery of iron-based superconductors in 2008, such as LaOFeAs [1] (1111-type), $BaFe_2As_2$ [2] (122-type), and α-FeSe(Te)(11-type) [3], as well as iron selenide, $K_xFe_{2-y}Se_2$ [4], the pairing mechanism for these materials and the search for high-transition temperature superconductors have attracted substantial interest. These compounds exhibit superconductivity after doping or under high pressures. Like cuprates, they share the same robust tetrahedral layered structure. Given the magnetic orders of their parent compounds, these compounds are in spin-density-wave (SDW) order and have collinear [5, 6], bicollinear [7–9], and block antiferromagnetic (AFM) structures [10–13] when contained in iron pnictides, iron chalcogenide, and iron selenide $K_xFe_{2-y}Se_2$, respectively, at temperatures below a tetragonal-orthorhombic structural transition temperature.

In addition to the presence of phase separation in $K_xFe_{2-y}Se_2$ [14–20], it has generated considerable experimental and theoretical interest. In particular, the scanning tunneling microscopy (STM) measurements obtained from $K_xFe_{2-y}Se_2$ clearly demonstrate phase separation [17, 18], which suggests that it is phase separated into iron-vacancy ordered regions and iron-vacancy free regions. In this case, the former regions insulate with a $\sqrt{5} \times \sqrt{5}$ vacancy ordered pattern, whereas the latter region is superconducting. Furthermore, neutron scattering experiments reveal that the $\sqrt{5}\times\sqrt{5}$ vacancy ordered phase is also AFM ordered [10], which is affected by the superconducting pairing [21]. Understanding this observation is difficult in terms of phase separation. In addition to the $\sqrt{5}\times\sqrt{5}$ vacancy ordered phase, an insulating phase with a $\sqrt{2} \times \sqrt{2}$ ordered pattern on the Fe layer was also observed [15, 16, 22, 23], which indicates the existence of an additional symmetry breaking order in the SC phases [17, 18, 24] using both STM [17, 18] and angle-resolved photoemission spectroscopy (ARPES) [24].

Theoretically, one author proposed [13] that the ground state of the alkali-doped iron selenide without iron vacancies should approach a checkerboard phase, in which each of the four Fe sites combine into a tetragonal structure. However, the interplay between magnetism and superconductivity remains unclear in $K_xFe_{2-y}Se_2$. Chemically, $K_xFe_{2-y}Se_2$ appears to be the most heavily electron-doped iron-based superconductor. This significantly differs from other iron-based superconductors,

which have both hole-like and electron-like Fermi surfaces [25–27] in the Brillouin zone. In order to examine the common aspects of the electronic structure and pairing mechanism of the iron-based systems that have the most electron-doped end, we considered the electronic and magnetic structures found in the isovalent-substituted compound KFe_2Te_2, using the framework of density functional theory, as the keys to an initial understanding of the possible superconducting mechanism.

In this paper, we present theoretical results concerning the electronic and magnetic structures of the ground state of KFe_2Te_2, which are obtained using intensive first-principle calculations. Similar calculations were partially provided in Ref. [28]. We reveal that weak spin fluctuation instability appears at momentum $\vec{q} = (\pi, \pi/2, 0)$, indicating that the ground state for KFe_2Te_2 has a bicollinear AFM structure, which is confirmed using magnetic state calculations. Further calculations demonstrate that there is a strong competition among the nearest, next-nearest, and next-next-nearest neighbor exchange interactions between the Fe local moments that are mediated by Te $5p$ orbitals. The exchange coupling is also evaluated, yielding the same magnitude. This magnetic competition strongly affects the electronic structure of KFe_2Te_2, producing a small orthorhombic lattice distortion and a bicollinear AFM order of the Fe moments, which are similar to those found in α-FeTe [7] and KFe_2Se_2 [29].

2 Structure and method

We perform first-principle calculations on KFe_2Te_2 and demonstrate that the electronic structure of parent KFe_2Te_2 can be regarded as an electron over-doped 11-type system, rather than on $BaFe_2As_2$, which is structurally much more similar [2]. This can be seen in Fig. 1(a). In our calculations, we used the projected augmented wave method [30], which was implemented in the VASP code [31], and the Perdew–Burke–Ernzerhof (PBE) exchange correlation potential [32]. All atomic positions and lattice constants were simultaneously relaxed in order to determine the ground state with space group $I4/mmm$. A 500 eV cutoff in the plane wave expansion ensures that the calculations converge to 10^{-5} eV. Moreover, the atomic positions and lattice constants were optimized until the largest force on any atom was 0.005 eV/Å. We used a $9 \times 9 \times 5$ Monkhorst–Pack k-grid Brillouin zone sampling throughout our calculations. Furthermore, in the calculation of the electronic and magnetic structures of the nonmagnetic (NM), ferromagnetic (FM), and square AFM Néel states, the $a \times a$ FeTe cell

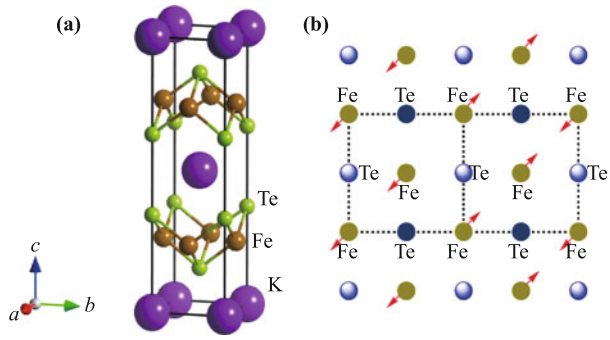

Fig. 1 **(a)** The schematically calculated crystal structure of the unit cell of KFe_2Te_2 containing two sandwiched FeAs layers. **(b)** Schematic top view of the FeTe layer. The large dashed square is $a \times 2a$ unit cell. The Fe spins in the bicollinear AFM order are shown by the red arrows.

was taken to be the base cell, and the unit cells were doubled. The base cells were the $\sqrt{2}a \times \sqrt{2}a$ and $a \times 2a$, as well as the 4×4 FeTe, cells for collinear, bicollinear, and block AFM states, respectively. The magnetic configuration of the bicollinear AFM state is shown in Fig. 1(b).

3 Results and discussion

First, we considered the electronic properties of KFe_2Te_2 in terms of their dependence on structural factors. Therefore, we performed a full structural optimization of KFe_2Te_2 for both the lattice parameters and atomic positions, including the internal coordinate, z_{Te}, of the Te atom using energy minimization. These results are summarized in Table 1. Here, we calculated five possible magnetic configurations using FM, square Néel AFM, collinear AFM, and bicollinear AFM, as well as the block AFM orders combined with the nonmagnetic states. The lattice parameters that were optimized in our NM calculations exceeded those for KFe_2Se_2, which suggests that the atomic radii of Te are larger than those of Se. In addition, our results agreed well with previous studies

Table 1 Geometry, energetic and magnetic properties of KFe_2Te_2. Results in columns of the FM, AFM, Colinear, and Bicollinear as well as Block AFM states correspond to their configurations using fully optimized structures, respectively. ΔE is the total energy difference per iron atom referenced to the fully optimized NM structure ($a = b = 4.0537$ Å, $c = 14.4722$ Å, and $z_{Te} = 0.3496$), and m_{Fe} is the local magnetic moment on Fe.

KFe_2Te_2	FM	AFM	Collinear	Bicollinear	Block
a (Å)	3.8876	4.0838	4.0522	3.8935	4.0421
b (Å)	3.8876	4.0838	4.0522	4.1044	4.0421
c (Å)	16.5437	14.9974	14.4937	15.8734	15.8564
z_{Te}	0.3586	0.3534	0.3494	0.3572	0.3579
ΔE (eV/Fe)	–0.2559	–0.1262	–0.1052	**–0.2750**	–0.2644
m_{Fe} (μ_B)	2.719	2.068	2.057	2.619	2.764

that applied the full-potential method [28].

Second, we examined the NM state of KFe_2Te_2. In other words, the spin degrees were not included in the calculation. This work can provide a reference for studying magnetization states. Analyzing the density of states (DOS) at the Fermi level lets us determine whether the magnetic state is preferred. Figure 2(a) displays the calculated total DOS, as well as the projected DOS (PDOS) calculations performed on the Fe 3*d* and Te 5*p* orbitals of KFe_2Te_2. The total DOS and PDOS of KFe_2Te_2 resemble those of KFe_2Se_2 systems [29, 33] and exhibit the typical characteristics of layered structures, which can also be seen in the Fermi surface topology in Fig. 2(c). Here, the DOS can be divided into two parts: the lower part (3 eV below the Fermi energy), which consists of the bands formed through the bonding of the Fe 3*d* and Te 5*p* orbitals, and the upper part, which basically contains the Fe 3*d* orbital bands ranging from −2 eV to 2 eV that are centered at the Fermi energy. Further examination of the PDOS data reveals that more than 95% of the states from −2.0 eV to 0 eV are from Fe 3*d* orbitals and that the Fe 3*d*/Te 5*p* orbital substantially hybridizes, ranging from −6.0 eV to 2.0 eV. Thus, we expect Fe 3*d* electrons to play a dominant role in conduction, which is mediated by Te 5*p* orbitals.

Furthermore, it should be noted that the DOS provided by the Fe 3*d* orbitals produces a large value at the Fermi level. The corresponding value of the DOS at the Fermi level is $N_{\mathrm{Fe}}(E_f) = 1.24$ states per eV per Fe atom. According to the Stoner criterion [34, 35], while magnetism may occur with lower DOS values, it must occur within a band picture if the Stoner criterion, $N(E_f)I > 1$, is met. Here, I represents the Stoner parameter, which assumes values between 0.7 and 0.9 eV for ions near the center of the 3*d* series. In this case, the NM state becomes unstable. Also, we should note that effective I can be reduced using hybridization. Therefore, the NM state is unstable against the magnetic states in the FeTe layer. On the other hand, the low energy band structure and its corresponding Fermi surface, which are shown in Figs. 1(b) and (c), respectively, demonstrate that KFe_2Te_2 is a highly electron-doped compound when compared with iron-pnictides [25, 26]. The result of this is a diminished hole pocket at the zone center and an enlarged electron pocket at the zone corner, which exhibits quite two dimensionality arisen from the nature of sandwiched FeTe layered structure.

Before exploring the ground state with magnetic order, we calculated the bare electron susceptibility, $\chi_0(\vec{q})$, which provides a signature with magnetic instability at momentum $\vec{q}$. Applying the tight-binding model, which is fitted using maximally localized Wannier functions [36, 37], the bare electron susceptibility is given by

$$\chi_0(\vec{q}) = \frac{1}{N_{\boldsymbol{k}}} \sum_{\mu\nu\boldsymbol{k}} \frac{|\langle \boldsymbol{k}+\vec{q},\mu|\boldsymbol{k},\nu\rangle|^2}{E_{\mu,\boldsymbol{k}+\vec{q}} - E_{\nu,\boldsymbol{k}} + i0^+} [f(E_{\nu,\boldsymbol{k}}) - f(E_{\mu,\boldsymbol{k}+\vec{q}})],$$

where $E_{\mu,\boldsymbol{k}}$ represents the band energy measured at Fermi level E_F, and $f(E_{\mu,\boldsymbol{k}})$ is the Fermi-Dirac distribution function for an eigenstate, $|\boldsymbol{k},\mu\rangle$. In addition, $N_{\boldsymbol{k}}$ denotes the number of $\boldsymbol{k}$ points used for the irreducible Brillouin zone integration. The calculated real part of χ_0 is found in Fig. 1(d). Here, we see that the highly electron dopant induced small peak appears at momentum $\vec{q} = (\pi, \pi/2, 0)$, which indicates the presence of a weak AFM spin fluctuation in the FeTe plane. In other words, the peak in bare electron susceptibility $\chi_0(\vec{q})$ suggests that the ground state of KFe_2Te_2 has a bicollinear AFM structure.

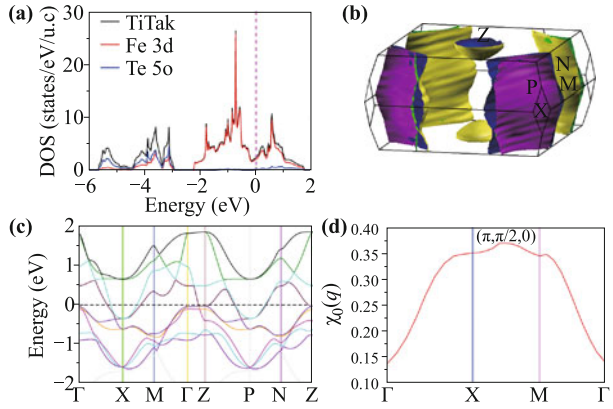

Fig. 2 **(a)** Total DOS and PDOS on Fe 3*d* and Te 5*p* orbitals of the NM state for KFe_2Te_2. **(b)** Energy band structure and **(c)** its corresponding Fermi surface topology for the NM state of KFe_2Te_2. **(d)** The real part of bare electron susceptibility $\chi_0(q)$. The Fermi energies are set to zero.

In order to analyze the magnetic instability along momentum $\vec{q} = (\pi, \pi/2, 0)$, which was indicated by the bare electron susceptibility, $\chi_0(\vec{q})$, we calculated five additional possible magnetic states using FM, square Néel AFM, collinear AFM, bicollinear AFM, and block AFM orders. These are listed in Table 1. If the energy for the NM state is set to zero, the ground state of KFe_2Te_2 has a bicollinear AFM order, in which the Fe moments ferromagnetically align along a diagonal direction and antiferromagnetically align along the other diagonal direction on the Fe-Fe square, as is shown in Fig. 1(b). Furthermore, the Fe local moments ($\sim 2.6\mu_B$), which are close to those of KFe_2Se_2 (with Fe local moments $\sim 2.5\mu_B$) [29], are also similar to those of α-FeTe [7]. The magnetic moment around each Fe atom is approximately $2.1\mu_B$–$2.7\mu_B$, weakly varying in our five magnetically ordering states. Given the bicollinear AFM structure, our

calculations indicate a small structure distortion, which diminishes along the spin-parallel alignment [y-axis in Fig. 1(a)] and expands along the spin-antiparallel alignment [x-axis in Fig. 1(a)], causing a structural transition from a tetragonal structure to an orthorhombic one. This readily implies that the direct exchange favors a shorter Fe-Fe separation, whereas the superexchange favors a longer Fe-Fe separation.

In order to quantify the magnetic interactions, we assume that the energy differences between these magnetic orders are predominantly due to the local exchange interactions between the Fe moments with spin $\vec{S}$, which can be effectively modeled by the following frustrated Heisenberg model [38], with respective nearest, next-nearest, and next-next-nearest neighbor couplings J_1, J_2, and J_3:

$$\hat{H} = J_1 \sum_{\langle i,j \rangle} \vec{S}_i \cdot \vec{S}_j + J_2 \sum_{\langle\langle i,j \rangle\rangle} \vec{S}_i \cdot \vec{S}_j + J_3 \sum_{\langle\langle\langle i,j \rangle\rangle\rangle} \vec{S}_i \cdot \vec{S}_j. \quad (1)$$

Here, $\langle i,j \rangle$, $\langle\langle i,j \rangle\rangle$, and $\langle\langle\langle i,j \rangle\rangle\rangle$ denote the summation over the nearest, next-nearest, and next-next-nearest neighboring sites, respectively. This model may overlook some contributions from the itinerant electrons; however, we believe it captures the general physics of the magnetic structures. From the calculated energy data listed in Table 1, we see that [7, 39], for KFe_2Te_2, we have $J_1 = -8.1$ meV/S^2, $J_2 = -5.37$ meV/S^2, and $J_3 = 7.93$ meV/S^2. It should be noted that these magnetic exchange constants have relatively smaller values than those found in other iron-based materials [23] because the magnetic ordering is gradually suppressed by the electron doped in pristine KFe_2Te_2, which results in weak magnetic fluctuations. This also agrees with the calculation of susceptibility $\chi_0(\vec{q})$ shown in Fig. 2(d). In addition, these values indicate that strong competing exchange interactions exist between the Fe spins. The bicollinear AFM has less energy than the other configurated AFM states for a frustrated J_1–J_2–J_3 Heisenberg model in terms of $J_3 > J_2/2$ and $J_2 > J_1/2$.

Finally, we calculated the low energy band structure and the total DOS, as well as the projected DOS, for Fe 3d and Te 5p, given the bicollinear AFM state in KFe_2Te_2, which can be seen in Fig. 3. When compared with the NM phase shown in Fig. 2(a), we find that most of the states around the Fermi level are gapped by the bicollinear AFM order. The corresponding electronic DOS at the Fermi level is $N(E_f) = 0.448$ states per eV per Fe atom, which is significantly less than that of the NM state (1.24 states per eV per Fe atom), as is intuitively expected. In addition, the stability of the obtained bicollinear AFM state in KFe_2Te_2 can be understood given the nature of the Fe-Te-Fe bond angle in iron-based materials [35], which uniquely determines the tetrahedral crystal environment and the competing orders between the orbital and lattice degrees of freedom. In KFe_2Te_2, the Fe-Te-Fe bond angle decreases to a small value (approximately 94.57°) because of the large radii of the Te atom, which enhance the direct FM interactions between the nearest neighbor Fe spin and the third-nearest neighbor superexchange interaction mediated by the Te 5p orbitals. This behavior is consistent with our calculated exchange coupling constants. Furthermore, the weak peak appearing in the spin susceptibility at momentum $\vec{q} = (\pi, \pi/2, 0)$ in Fig. 1(d) not only suggests the presence of SDW in the FeTe layer but also implies the tight relation between superconductivity and spin fluctuation. Clarifying the role of this relationship may provide insight concerning the mechanism of superconductivity that is driven by electron-electron correlation [40]. We aim to address this issue in future studies.

4 Conclusions

We performed first-principle calculations for the study of the electronic and magnetic structures of KFe_2Te_2. Our

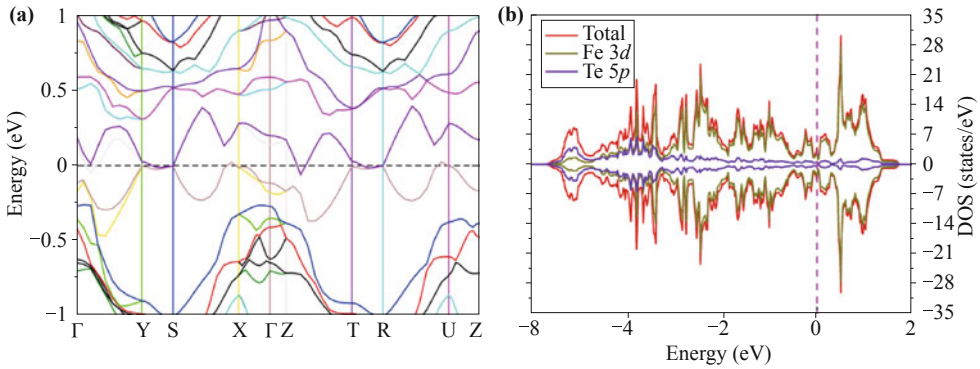

Fig. 3 **(a)** The low energy band structure and **(b)** total DOS and PDOS on Fe 3d and Te 5p orbitals for the bicollinear AFM state for KFe_2Te_2. The Fermi energies are set to zero.

numerical calculations suggest that spin fluctuation instability appears at momentum $\vec{q} = (\pi, \pi/2, 0)$, which indicates that the ground state for KFe_2Te_2 has a bicollinear AFM structure. This is consistent with magnetic states calculations. Furthermore, we also determined a strong competition among nearest, next-nearest, and next-next-nearest neighbor exchange interactions between Fe local spins mediated by Te $5p$ orbitals, providing the bicollinear AFM order of Fe spins in the ground states that have a magnetic moment of $\sim 2.6\mu_B$ around each Fe atom. This discovery may provide some understanding of the interplay between magnetism and superconductivity in the family of iron-based materials.

Acknowledgements We thank R. B. Tao, C. S. Ting, Y. Chen, J. P. Hu, D. L. Feng, M. H. Jiang, X. M. Xie, Z. Liu, D. W. Shen, and G. Mu for their helpful discussion. This work was supported by the Strategic Priority Research Program (B) of the Chinese Academy of Sciences (Grant No. XDB04040300), the National Natural Science Foundation of China (Grant Nos. 11227902 and 11404359), and Shanghai Yang-Fan Program (Grant Nos. 14YF1407100 and 14YF1407000).

References

1. Y. Kamihara, T. Watanabe, M. Hirano, and H. Hosono, Iron-based layered superconductor $La[O_{1-x}F_x]FeAs$ (x = 0.05–0.12) with T_c = 26 K, *J. Am. Chem. Soc.* 130(11), 3296 (2008)
2. M. Rotter, M. Tegel, D. Johrendt, I. Schellenberg, W. Hermes, and R. Pöttgen, Spin-density-wave anomaly at 140 K in the ternary iron arsenide $BaFe_2As_2$, *Phys. Rev. B* 78(2), 020503 (2008)
3. F. C. Hsu, J. Y. Luo, K. W. Yeh, T. K. Chen, T. W. Huang, P. M. Wu, Y. C. Lee, Y. L. Huang, Y. Y. Chu, D. C. Yan, and M. K. Wu, Superconductivity in the PbO-type structure a-FeSe, *Proc. Natl. Acad. Sci. USA* 105(38), 14262 (2008)
4. J. Guo, S. Jin, G. Wang, S. Wang, K. Zhu, T. Zhou, M. He, and X. Chen, Superconductivity in the iron selenide $K_xFe_2Se_2$ ($0 \leqslant x \leqslant 1.0$), *Phys. Rev. B* 82, 180520(R) (2010)
5. C. de la Cruz, Q. Huang, J. W. Lynn, J. Li, W. R. Ii, J. L. Zarestky, H. A. Mook, G. F. Chen, J. L. Luo, N. L. Wang, and P. Dai, Magnetic order close to superconductivity in the iron-based layered $LaO_{1-x}F_xFeAs$ systems, *Nature* 453 (7197), 899 (2008)
6. J. Dong, H. J. Zhang, G. Xu, Z. Li, G. Li, W. Z. Hu, D. Wu, G. F. Chen, X. Dai, J. L. Luo, Z. Fang, and N. L. Wang, Competing orders and spin-density-wave instability in $La(O_{1-x}F_x)FeAs$, *Europhys. Lett.* 83(2), 27006 (2008)
7. F. Ma, W. Ji, J. Hu, Z. Y. Lu, and T. Xiang, First-principles calculations of the electronic structure of tetragonal α-FeTe and α-FeSe crystals: Evidence for a bicollinear antiferromagnetic order, *Phys. Rev. Lett.* 102(17), 177003 (2009)
8. S. Li, C. de la Cruz, Q. Huang, Y. Chen, J. W. Lynn, J. Hu, Y. L. Huang, F. C. Hsu, K. W. Yeh, M. K. Wu, and P. Dai, First-order magnetic and structural phase transitions in $Fe_{1+y}Se_xTe_{1-x}$, *Phys. Rev. B* 79(5), 054503 (2009)
9. W. Bao, Y. Qiu, Q. Huang, M. A. Green, P. Zajdel, M. R. Fitzsimmons, M. Zhernenkov, S. Chang, M. Fang, B. Qian, E. K. Vehstedt, J. Yang, H. M. Pham, L. Spinu, and Z. Q. Mao, Tunable $(\delta\pi, \delta\pi)$-type antiferromagnetic order in α-Fe(Te,Se) superconductors, *Phys. Rev. Lett.* 102(24), 247001 (2009)
10. W. Bao, Q. Z. Huang, G. F. Chen, D. M. Wang, J. B. He, X. Q. Wang, and Y. Qiu, A novel large moment antiferromagnetic order in $K_{0.8}Fe_{1.6}Se_2$ superconductor, *Chin. Phys. Lett.* 28(8), 086104 (2011)
11. C. Cao and J. Dai, Block spin ground state and three-dimensionality of $(K,Tl)_yFe_{1.6}Se_2$, *Phys. Rev. Lett.* 107(5), 056401 (2011)
12. X. W. Yan, M. Gao, Z. Y. Lu, and T. Xiang, Ternary iron selenide $K_{0.8}Fe_{1.6}Se_2$ is an antiferromagnetic semiconductor, *Phys. Rev. B* 83(23), 233205 (2011)
13. W. Li, S. Dong, C. Fang, and J. Hu, Block antiferromagnetism and checkerboard charge ordering in the alkali-doped iron selenides $R_{1-x}Fe_{2-y}Se_2$, *Phys. Rev. B* 85, 100407(R) (2012)
14. C. H. Li, B. Shen, F. Han, X. Zhu, and H. H. Wen, Transport properties and anisotropy of $Rb_{1-x}Fe_{2-y}Se_2$ single crystals, *Phys. Rev. B* 83(18), 184521 (2011)
15. Y. J. Yan, M. Zhang, A. F. Wang, J. J. Ying, Z. Y. Li, W. Qin, X. G. Luo, J. Q. Li, J. Hu, and X. H. Chen, Electronic and magnetic phase diagram in $K_xFe_{2-y}Se_2$ superconductors, *Sci. Rep.* 2, 212 (2012)
16. F. Chen, M. Xu, Q. Q. Ge, Y. Zhang, Z. R. Ye, L. X. Yang, J. Jiang, B. P. Xie, R. C. Che, M. Zhang, A. F. Wang, X. H. Chen, D. W. Shen, M. H. Jiang, J. P. Hu, and D. L. Feng, Electronic identification of the parental phases and mesoscopic phase separation of $K_xFe_{2-y}Se_2$ superconductors, *Phys. Rev. X* 1(2), 021020 (2011)
17. P. Cai, C. Ye, W. Ruan, X. Zhou, A. Wang, M. Zhang, X. Chen, and Y. Wang, Imaging the coexistence of a superconducting phase and a charge-density modulation in the $K_{0.73}Fe_{1.67}Se_2$ superconductor using a scanning tunneling microscope, *Phys. Rev. B* 85(9), 094512 (2012)
18. W. Li, H. Ding, P. Deng, K. Chang, C. Song, K. He, L. Wang, X. Ma, J. P. Hu, X. Chen, and Q. K. Xue, Phase separation and magnetic order in K-doped iron selenide superconductor, *Nat. Phys.* 8(2), 126 (2011)
19. R. H. Yuan, T. Dong, Y. J. Song, P. Zheng, G. F. Chen, J. P. Hu, J. Q. Li, and N. L. Wang, Nanoscale phase separation of antiferromagnetic order and superconductivity in $K_{0.75}Fe_{1.75}Se_2$, *Sci. Rep.* 2, 221 (2012)
20. A. Zhang, T. Xia, K. Liu, W. Tong, Z. R. Yang, and Q. M. Zhang, Superconductivity at 44 K in K intercalated FeSe system with excess Fe, *Sci. Rep.* 3, 1216 (2013)
21. W. Bao, G. N. Li, Q. Huang, G. F. Chen, J. B. He, M. A. Green, Y. Qiu, D. M. Wang, and J. L. Luo, Superconductiv-

ity tuned by the iron vacancy order in $K_xFe_{2-y}Se_2$, *Chin. Phys. Lett.* 30(2), 027402 (2013)

22. Z. Wang, Y. J. Song, H. L. Shi, Z. W. Wang, Z. Chen, H. F. Tian, G. F. Chen, J. G. Guo, H. X. Yang, and J. Q. Li, Microstructure and ordering of iron vacancies in the superconductor system $K_yFe_xSe_2$ as seen via transmission electron microscopy, *Phys. Rev. B* 83(14), 140505 (2011)
23. D. X. Mou, L. Zhao, and X. J. Zhou, Structural, magnetic and electronic properties of the ironCchalcogenide $A_xFe_{2-y}Se_2$ (A = K, Cs, Rb, and Tl, etc.), *Front. Phys.* 6(4), 410 (2011)
24. D. Mou, S. Liu, X. Jia, J. He, Y. Peng, L. Zhao, L. Yu, G. Liu, S. He, X. Dong, J. Zhang, H. Wang, C. Dong, M. Fang, X. Wang, Q. Peng, Z. Wang, S. Zhang, F. Yang, Z. Xu, C. Chen, and X. J. Zhou, Distinct Fermi surface topology and nodeless superconducting gap in a $(Tl_{0.58}Rb_{0.42})Fe_{1.72}Se_2$ superconductor, *Phys. Rev. Lett.* 106(10), 107001 (2011)
25. I. I. Mazin, D. J. Singh, M. D. Johannes, and M. H. Du, Unconventional superconductivity with a sign reversal in the order parameter of $LaFeAsO_{1-x}F_x$, *Phys. Rev. Lett.* 101(5), 057003 (2008)
26. K. Kuroki, S. Onari, R. Arita, H. Usui, Y. Tanaka, H. Kontani, and H. Aoki, Unconventional pairing originating from the disconnected Fermi surfaces of superconducting $LaFeAsO_{1-x}F_x$, *Phys. Rev. Lett.* 101(8), 087004 (2008)
27. W. Li, J. Li, J. X. Zhu, Y. Chen, and C. S. Ting, Pairing symmetry in the iron-pnictide superconductor KFe_2As_2, *Europhys. Lett.* 99(5), 57006 (2012)
28. I. R. Shein and A. L. Ivanovskii, Structural, electronic properties and Fermi surface of $ThCr_2Si_2$-type tetragonal KFe_2S_2, KFe_2Se_2, and KFe_2Te_2 phases as parent systems of new ternary iron-chalcogenide superconductors, arXiv: 1102.4173 (2011)
29. X. W. Yan, M. Gao, Z. Y. Lu, and T. Xiang, Electronic and magnetic structures of the ternary iron selenides AFe_2Se_2 (A = Cs, Rb, K, or Tl), *Phys. Rev. B* 84(5), 054502 (2011)
30. P. E. Blöchl, Projector augmented-wave method, *Phys. Rev. B* 50(24), 17953 (1994)
31. G. Kresse and J. Furthmuller, Efficient iterative schemes for *ab initio* total-energy calculations using a plane-wave basis set, *Phys. Rev. B* 54(16), 11169 (1996)
32. J. P. Perdew, K. Burke, and M. Erznerhof, Generalized gradient approximation made simple, *Phys. Rev. Lett.* 77(18), 3865 (1996)
33. C. Cao and J. Dai, Electronic structure of KFe_2Se_2 from first-principles calculations, *Chin. Phys. Lett.* 28(5), 057402 (2011)
34. D. J. Singh, Electronic structure and doping in $BaFe_2As_2$ and LiFeAs: Density functional calculations, *Phys. Rev. B* 78(9), 094511 (2008)
35. W. Li, J. X. Zhu, Y. Chen, and C. S. Ting, First-principles calculations of the electronic structure of iron-pnictide $EuFe_2(As,P)_2$ superconductors: Evidence for antiferromagnetic spin order, *Phys. Rev. B* 86(15), 155119 (2012)
36. N. Marzari and D. Vanderbilt, Maximally localized generalized Wannier functions for composite energy bands, *Phys. Rev. B* 56(20), 12847 (1997)
37. A. A. Mostofi, J. R. Yates, Y. S. Lee, I. Souza, D. Vanderbilt, and N. Marzari, Wannier90: A tool for obtaining maximally-localised Wannier functions, *Comput. Phys. Commun.* 178(9), 685 (2008)
38. W. Li, C. Setty, X. H. Chen, and J. Hu, Electronic and magnetic structures of chain structured iron selenide compounds, *Front. Phys.* 9(4), 465 (2014)
39. F. Ma, Z. Y. Lu, and T. Xiang, Arsenic-bridged antiferromagnetic superexchange interactions in LaFeAsO, *Phys. Rev. B* 78(22), 224517 (2008)
40. Y. Liang, X. Wu, W. F. Tsai, and J. P. Hu, Pairing symmetry in layered BiS_2 compounds driven by electron-electron correlation, *Front. Phys.* 9(2), 194 (2014)